Switchblade: An Agile Treaded Rover

Nicholas Morozovsky, Christopher Schmidt-Wetekam, Thomas Bewley

***Abstract*— A versatile unmanned ground vehicle (UGV) should be able to traverse rough terrain while retaining a small form factor for navigating confined spaces. Such a (patent pending) vehicle, dubbed Switchblade, is developed in the present work via an effective combination of a novel transforming mechanical design, capable onboard electronics, and advanced feedback control algorithms. A single chassis holds the actuators, sensors, electronics, and battery. Shafts protruding from either side of this chassis connect to tread assemblies. Rotation of this shaft causes the treads to advance for translational movement; rotation about this shaft causes the entire tread assembly to rotate with respect to the chassis. Vehicle orientation is estimated via onboard filtering of optical encoders and MEMS accelerometers and gyros. In its horizontal configuration, Switchblade operates as a differential-drive treaded platform. In its various upright configurations, Switchblade operates as a mobile inverted pendulum, capable of surmounting obstacles, including stairs, that would otherwise be impassable by a vehicle of its size. Design-for-manufacturing (DFM) and design-for-assembly (DFA) techniques are employed to reduce cost, part count, complexity, and assembly time without sacrificing system capabilities. Results from a working prototype are discussed. The resulting platform is well suited for a variety of socially-relevant applications, including reconnaissance, mine exploration, and search & rescue.**

I. Introduction

A number of applications motivate small, simple UGVs that can robustly overcome complex terrain challenges, while also being able to navigate in confined spaces; such applications include patrol, search & rescue, mine exploration, and the disposal of improvised explosive devices (IEDs). In such applications, it is generally advantageous for the vehicles used to be inexpensive, so that multiple vehicles may be deployed to accomplish a given mission, and the loss of some is acceptable. The cost of a UGV may be reduced by minimizing its size and mechanical complexity, noting that advanced feedback control algorithms, once designed, may generally be implemented at low cost.

Inverted pendula are often used in controls labs as a fundamental teaching tool. In recent years, mobile inverted pendula have become increasingly popular, including the Segway Personal Transporter [1]. The Segway is perhaps the only mobile inverted pendulum to have yet ventured outside of the sheltered lab environment on a large scale, and is itself largely operated on flat sidewalks.

We begin by reviewing existing mobile inverted pendula. The most common paradigm today is a two-wheeled platform ([2], [3]), with steering accomplished by differential drive. Another class of mobile inverted pendula uses a single ball instead of two wheels, thereby achieving holonomic locomotion ([4], [5]). Both designs have a fundamental weakness in common: the maximum obstacle size that such a vehicle can overcome is limited by the diameter of its wheels or ball.

All three authors are affiliated with the Coordinated Robotics Lab, University of California San Diego, La Jolla, CA 92093-0411 USA; e-mail: nmorozov@ucsd.edu, cmschmid@ucsd.edu, bewley@ucsd.edu

Fig. 1: Completed Switchblade prototype.

Legged robots often use a linear inverted pendulum model and calculations of the zero moment point to maintain balance while stationary or moving [6]. Such robots have a great deal of flexibility when overcoming obstacles: they may step over or onto an obstacle [7], or even hop over an obstacle [8]; however, they are also mechanically complex, with many actuators and possible failure points.

The standard treaded platform (manned versions of which were developed by the British in WW1, and smaller unmanned versions of which were developed by the Germans in WW2) consists of two fixed tread mechanisms mounted on opposite sides of a central chassis. This type of UGV performs well over a variety of both smooth and rough terrain (including loose dirt and gravel, sand, snow, mud, etc.), but cannot generally overcome obstacles larger than the diameter of its tread sprocket. This limitation may be extended by adding additional idler sprockets to increase the height of the tread assembly (such as the trapezoidal shape of the treads of an M1 Abrams tank), or by adding secondary articulated treaded segments or "flippers" (e.g., the iRobot PackBot [9]). Additional treaded segments may be added to increase a treaded vehicle's agility [10], but at the expense of significantly increased cost, complexity, and possible failure points; for instance, a serpentine robot may consist entirely of treaded segments [11].

Another notable treaded platform is the Vecna Robotics Battlefield Extraction-Assist Robot (BEAR; see [12]), which

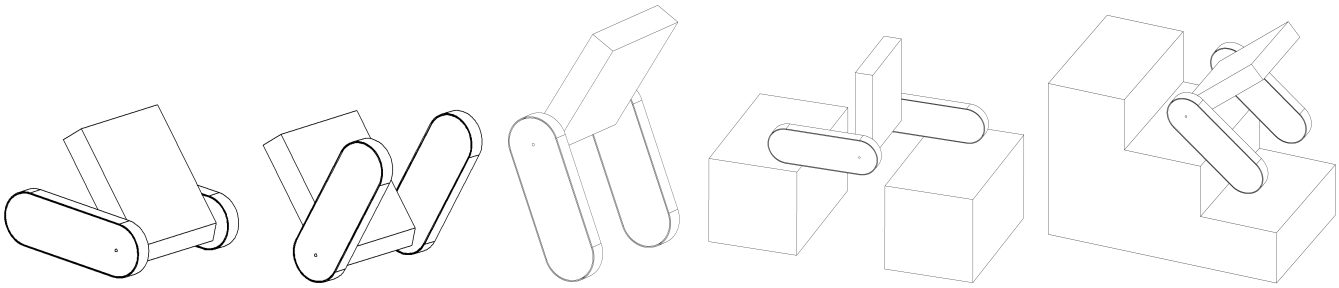

(a) Horizontal (b) V-balance mode (c) C-balance mode (d) Chasm crossing (e) Perching on an edge

Fig. 2: Different operating modes of the Switchblade design.

has two-segment tread assemblies pivotally attached to either side of a central torso which also has two manipulator arms. The BEAR can operate with its articulated tread assemblies in a number of different configurations, including dynamically balancing on either end of the tread assemblies with inverted pendulum control. Note that the BEAR is a large, complex vehicle, with tread segments large enough to overcome many common obstacles (stairs, medium-sized rubble, etc.) without utilizing balancing behavior.

In this paper, we describe a (patent pending) compact treaded UGV, dubbed Switchblade, which is capable of overcoming obstacles nearly as high as its treads are long via a unique mechanical architecture and clever implementation of feedback control algorithms (Fig. 1). We first discuss the mechanical design of the platform and some of the static and dynamic maneuvers of which this platform is capable. Next, we describe one of the maneuvers in detail, deriving the dynamics and designing a controller. Finally, we present a working prototype in detail and conclude with the future work for this platform.

II. Architecture & Maneuvers

As in a traditional treaded vehicle, Switchblade has a pair of tread assemblies, driven by an internal sprocket, mounted on either side of a central chassis (Fig. 2a). Uniquely, the tread assemblies can rotate continuously about the main drive axle of the chassis. Changing the angle between the chassis and tread assemblies moves the center of mass. There are no physical connections between the two tread assemblies to keep them parallel, but feedback control may be applied when it is desired to keep the two tread assemblies in line.

In a horizontal configuration (Fig. 2a) the robot functions much like any other treaded skid-steer robot, with the ability to independently drive each tread forward or backward to drive and turn. The treads act to minimize contact force on loose surfaces and maintain traction better than wheels. Note that the actuated tread assemblies make the robot impervious to high-centering. Note also that the robot operates just as easily "upside down" as "right side up." Driving over rough terrain may induce unwanted vibration in the chassis, this vibration can be reduced by pivoting the chassis in response to a disturbance. Given the nature of the coupled system, the greatest disturbance rejection is realizable at the end of the chassis farthest from the pivoting axis. One application of such an active suspension system is image stabilization for a camera mounted in or on the chassis.

The robot may balance on either end of the treads by taking advantage of the tread transferring torque to the idler sprocket. In a wheeled design, the idler wheel would be passive unless a second motor was driving it or if a chain or belt connected the front and rear wheels. When the robot is balancing on the sprockets coaxial with the pivoting axis, a side view of the robot resembles the letter "V" (Fig. 2b), this maneuver is referred to as V-balance mode. Alternatively, the robot may balance on the distal sprockets of the treads, a side view of which resembles a crude version of the letter "C" (Fig. 2c), this is called C-balance mode. By driving the treads, rotating the angle of the tread assemblies, or actuating both simultaneously, the robot is able to maintain its balance.

Unlike the canonical inverted pendulum, the unstable equilibrium point (the angle of the chassis with respect to gravity at which the center of mass is directly over the contact point with the ground) is not constant and instead depends on the angle of the tread assemblies with respect to the chassis, and their relative mass distributions. This angle can be calculated with the known properties of the vehicle. There are multiple maneuvers, some dynamic and some quasi-static, for transitioning between the horizontal configuration and the upright configurations. One such maneuver for uprighting into V-balance mode will be discussed in section IV.

The maximum height of the robot in V-balance mode is the length of the treads with the center of mass approximately central, whereas in C-balance mode, the maximum height is the length of the chassis plus the length of the tread assemblies minus the radius of the sprocket, with the center of mass above the treads. The added height in C-balance mode allows the robot to stand up taller, climb larger obstacles, and to see farther with the onboard camera. The ground clearance of the chassis can be nearly the length of the tread assemblies, allowing the robot to pass over minor obstacles.

The separation angle between the chassis and the tread assemblies is hereafter referred to as the V-angle. The maximum V-angle achievable in V-balance mode is dependent on the mass properties of the tread assemblies and chassis and is less than or equal to 180°. In the present design, the tread assemblies are longer than the chassis, such that the

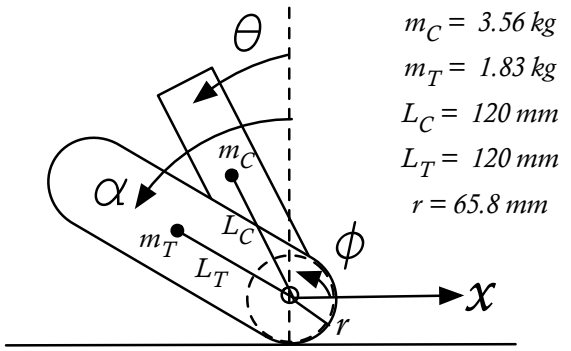

Fig. 3: Coordinate system for V-balance mode and parameters.

chassis may rotate continuously and pass through the tread assemblies while in C-balance mode.

The maximum obstacle size that the robot can overcome is related to its overall height. When the robot is horizontal, its height is the diameter of the tread sprocket; when the robot is upright, its height is related to the tread length. The total height of the robot is thus variable over a large range, and can be adjusted as necessary: the robot can upright itself to overcome large obstacles, then lay itself back down to, e.g., pass freely underneath parked cars.

To overcome an obstacle larger than the sprocket diameter, the robot approaches the obstacle while balancing upright, "leans" onto the obstacle by shifting its center of mass over the point of contact with the obstacle, then drives over the obstacle. An alternative maneuver to climb stairs uses the chassis of the robot as a lever. The robot approaches the step in a horizontal configuration, and rotates the chassis against the step; leveraging against this contact point appropriately while driving the treads, the center of mass may be pushed on top of the step. The tread assemblies may then be rotated up onto the step. After these moves, the robot is backwards relative to how it approached the step; to climb additional steps, the robot must reorient itself. If the length of the robot is less than the length of the step, the robot can flip itself in place on the step. The entire sequence can be repeated to climb multiple steps.

Using the independent nature of the tread assemblies, the robot may drive over a chasm or ditch nearly as wide as the tread assembly is long. The tread assemblies are rotated 180° apart and the chassis is positioned vertically, such that the center of mass is centered above the main drive axle (Fig. 2d). Balancing over a chasm is another unstable equilibrium; dynamic stabilization about the roll axis is accomplished by pivoting the tread assemblies to tilt the chassis side-to-side.

A particularly advanced, and challenging, maneuver is balancing on an edge, such as the edge of a step (Fig. 2e). Maintaining traction is critical; the material and shape of the treads and edge determine the critical slip angle. The contact angle can be controlled to a value less than this. Ultimately, the robot may drive up a step, contacting only the edge, while pivoting the chassis to keep the center of mass directly over the edge. This maneuver may be repeated up a staircase depending on the rise and pitch angle of the stairs, the length of the treads, and the critical slip angle.

The first maneuver we chose to develop was V-balance mode; the dynamics and control of this maneuver will be described in detail next.

III. Dynamics

By symmetry, we simplify the model to three bodies in two dimensions, the angles are defined in Fig. 3, where θ and α are the angles of the chassis and tread assembly from vertical respectively, ϕ is the rotation angle of the tread sprocket, and x is the horizontal position of the robot. Motors on the robot may exert torques along the axis of rotation between the tread sprocket and the chassis and between the chassis and the tread assembly.

The kinetic energies of the sprocket, chassis, and tread assembly are given respectively by

$$T_S = \frac{1}{2}\left[m_S\dot{x}^2 + J_S\dot{\phi}^2\right],$$

$$T_C = \frac{1}{2}\left[m_C\left(\dot{x} - L_C\dot{\theta}\cos\theta\right)^2 + m_C\left(L_C\dot{\theta}\sin\theta\right)^2 + J_C\dot{\theta}^2\right],$$

$$T_T = \frac{1}{2}\left[m_T\left(\dot{x} - L_T\dot{\alpha}\cos\alpha\right)^2 + m_T\left(L_T\dot{\alpha}\sin\alpha\right)^2 + J_T\dot{\alpha}^2\right].$$

The gravitational potential energy is given by

$$V = m_C g L_C\cos\theta + m_T g L_T\cos\alpha.$$

We define the generalized coordinates as

$$q = \begin{pmatrix} x & \phi & \alpha & \theta \end{pmatrix}^T.$$

The Lagrangian can be written as $\mathcal{L} = T_S + T_C + T_T - V$. By solving the Euler-Lagrange equations, we can write the equations of motion in the form

$$M(q)\ddot{q} + F(q,\dot{q}) = B\tau, \tag{1}$$

where the τ vector represents the control input torques for motors located in the robot's chassis. The first element represents the motor torque between the chassis and the tread sprocket and the second element represents the motor torque between the chassis and the tread assembly. Note also that:

$$M(q) = \begin{bmatrix} m_S + m_C + m_T & 0 & -m_T L_T\cos\alpha & -m_C L_C\cos\theta \\ 0 & J_S & 0 & 0 \\ -m_T L_T\cos\alpha & 0 & m_T L_T^2 + J_T & 0 \\ -m_C L_C\cos\theta & 0 & 0 & m_C L_C^2 + J_C \end{bmatrix}$$

$$F(q,\dot{q}) = \begin{pmatrix} m_C L_C\dot{\theta}^2\sin\theta + m_T L_T\dot{\alpha}^2\sin\alpha \\ 0 \\ -m_T g L_T\sin\alpha \\ -m_C g L_C\sin\theta \end{pmatrix},$$

$$B = \begin{bmatrix} 0 & 0 \\ 1 & 0 \\ 0 & 1 \\ -1 & -1 \end{bmatrix}.$$

We next impose a no-slip constraint between the tread sprocket and the ground, which will be shown also achieves a coordinate reduction, via

$$x + r\phi = 0, \tag{2}$$

or equivalently

$$A\dot{q} = 0, \quad A = \begin{pmatrix} 1 & r & 0 & 0 \end{pmatrix}.$$

In this system, A is not dependent on q. We append (1) with the inner product of the constraint matrix A with λ, the Lagrange multiplier:

$$M(q)\ddot{q} + F(q,\dot{q}) = B\tau + A^T\lambda. \tag{3}$$

A basis for the null space of A is given by

$$S = \begin{bmatrix} -r & 0 & 0 \\ 1 & 0 & 0 \\ 0 & 1 & 0 \\ 0 & 0 & 1 \end{bmatrix}. \tag{4}$$

Given that $\dot{q}$ is in this space, we define ν accordingly as

$$\dot{q} = S\nu, \quad \nu = \begin{pmatrix} \dot{\phi} & \dot{\alpha} & \dot{\theta} \end{pmatrix}^T. \tag{5}$$

Premultiplying by S^T and using (5), we can rewrite (3) as

$$S^T M(q) S\dot{\nu} + S^T F(q,\dot{q}) = S^T B\tau. \tag{6}$$

Noting that the dynamics of x and ϕ are directly coupled by (2), we can choose a reduced coordinate set $q_r = \begin{pmatrix} \phi & \alpha & \theta \end{pmatrix}^T$. Likewise truncating the top row of (4), $S_r = I_{3\times 3}$ and we see that $\dot{q}_r = \nu$ directly from (5).

Finally, we model the torque output τ from each motor linearly as

$$\tau = su - b\omega, \quad s = \frac{k\gamma V}{R}, \quad b = \frac{(k\gamma)^2}{R}, \tag{7}$$

where s is the stall torque, u is the control input (limited to $[-1, 1]$), b is the damping coefficient of the motor, ω is the speed of the motor shaft relative to the motor body, k is the motor constant, γ is the gear ratio of the transmission, V is the nominal voltage applied across the terminals, and R is the terminal resistance. Substituting the motor model, we can rewrite (6) using Rayleigh's dissipation function

$$S^T M(q) S\dot{\nu} + S^T F(q,\dot{q}) = S^T B[s\mathbf{u} - D(\dot{q})], \tag{8}$$

$$s = \begin{pmatrix} s_S & 0 \\ 0 & s_T \end{pmatrix}, \quad D(\dot{q}) = \begin{pmatrix} b_S(\dot{\phi} - \dot{\theta}) \\ b_T(\dot{\alpha} - \dot{\theta}) \end{pmatrix}.$$

Concatenating q_r and ν yields a complete state vector $\mathbf{x}$. Rewriting (8), we see that this nonlinear system is affine in the inputs:

$$\mathbf{x} = \begin{pmatrix} q_r \\ \nu \end{pmatrix}, \quad \dot{\mathbf{x}} = f(\mathbf{x}) + g(\mathbf{x})\mathbf{u},$$

$$f(\mathbf{x}) = \begin{pmatrix} \nu \\ -[S^T M(q) S]^{-1} S^T [F(q,\dot{q}) + BD(\dot{q})] \end{pmatrix},$$

$$g(\mathbf{x}) = \begin{pmatrix} 0_{3\times 2} \\ \left[S^T M(q) S\right]^{-1} S^T Bs \end{pmatrix}.$$

IV. Controller Design

A. Linearization and LQR

We begin by linearizing the system about the desired operating point, the unstable equilibrium with all states and control inputs equal to zero.

$$\dot{\mathbf{x}} = A\mathbf{x} + B\mathbf{u}, \quad A = \frac{\delta f}{\delta \mathbf{x}}\Big|_{\mathbf{x}=0}, \quad B = g(\mathbf{x})\Big|_{\mathbf{x}=0}. \tag{9}$$

A state feedback gain matrix K_c is found using the linear quadratic regulator (LQR) method. The weighting matrices are determined by Bryson's method:

$$Q_c = diag\left(\left[\frac{1}{(3\pi)^2}\ \frac{1}{(1/8)^2}\ \frac{1}{(1/8)^2}\ \frac{1}{(8\pi)^2}\ \frac{1}{(7/2)^2}\ \frac{1}{(7/2)^2}\right]\right)$$

$$R_c = diag\left(\left[\frac{1}{(1/4)^2}\ \frac{1}{(1/2)^2}\right]\right), \quad N_c = 0_{6\times 2}.$$

As noted, the motor model in (7) is valid for a bounded control input u, so each element from $\mathbf{u} = K_c\mathbf{x}$ is saturated at unity magnitude.

An important finding is that simply running the controller from certain statically stable positions (e.g. the tread assembly horizontal $\alpha = 90°$ and the chassis just past vertical $\theta = -15°$) is sufficient to upright and stabilize the robot, see Fig. 4. Given these initial conditions, the center of mass is near the end of the treads by the chassis (Fig. 4a), and the control law derived from LQR will drive the treads backwards (Fig. 4b), which will cause the robot to tip forwards leaving only the tread sprocket in contact with the ground (Fig. 4c). Simultaneously, the V-angle is reduced by actuation of the motors between the chassis and tread assemblies (Fig. 4d) and the treads are driven until the sprocket is back in the original position (Fig. 4e).

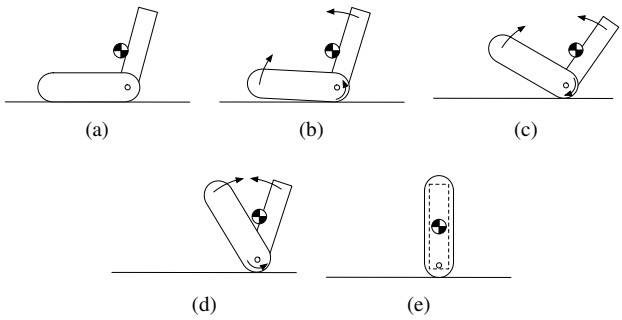

Fig. 4: Maneuver for uprighting into V-balance mode with LQR control with center of mass indicated.

B. Discretization

Since the control will be implemented with digital electronics, we must discretize the system; we choose a sample time of $h = 0.01s$. We convert our continuous-time system from (9) using the matrix exponential:

$$F = \Phi(h), \quad \Phi(\tau) = \mathbf{e}^{A\tau},$$
$$G = \Gamma(h), \quad \Gamma(\tau) = \int_0^\tau \mathbf{e}^{A\eta} B d\eta.$$

The continuous time weighting matrices are also transformed (given that $N_c = 0$):

$$Q_d = \int_0^h \Phi^T(\tau) Q_c \Phi(\tau) d\tau,$$
$$R_d = \int_0^h \Gamma^T(\tau) Q_c \Gamma(\tau) + R_c d\tau,$$
$$N_d = \int_0^h \Phi^T(\tau) Q_c \Gamma(\tau) d\tau.$$

A new state feedback matrix K_d is found using the discrete-time LQR method. Comparing the simulation results between the continuous-time and discrete-time state feedback controllers (both applied to the continuous-time dynamic model of the nonlinear plant) reveals negligible performance loss.

C. Estimation

On the physical system we are limited in what states can be observed based on available sensors. Thus we design an estimator to recreate the full state vector. The chassis of the robot is instrumented with MEMS accelerometers and gyroscopes and optical encoders. The gyroscope can measure the rotational velocity of the chassis providing a direct measurement of $\dot{\theta}$. The accelerometer outputs acceleration magnitudes in two orthogonal axes; by taking the arctangent of the two values, the gravity vector can be calculated, under the assumption that the body acceleration is small. Adding a low-pass filter improves noise attenuation. This method yields an acceptable estimate of θ at low frequencies.

Another method to estimate θ is to numerically integrate the output of the gyroscope. Integration error and thermal bias build over time, but can be eliminated using a high pass filter, thus creating an estimate of θ that is valid only at higher frequencies. Choosing the accelerometer low pass filter constant and integrated gyroscope high pass filter constant such that they sum to unity allows the two measurements to be combined for a single estimate of θ valid across a wide frequency range. The encoders precisely measure the relative rotation and rotational velocity between the chassis and the tread sprocket and between the chassis and the tread assembly. Given θ, $\dot{\theta}$, and the encoder data, ϕ, $\dot{\phi}$, α, and $\dot{\alpha}$ can be computed by simple addition.

For the purposes of simulation, we mimic the output of the sensors by manipulating the state vector. For the encoders, we simply quantize the simulation state given the resolution of the encoder. For the MEMS gyroscope and accelerometer, we calculate what the sensor output would be given the current state, and then add white noise, the variance of which is based on the manufacturer's specifications. Simulating the discrete-time controller using the estimated feedback again shows negligible performance loss as compared to continuous-time state feedback control. Simulation results for the uprighting maneuver can be seen in Fig. 6.

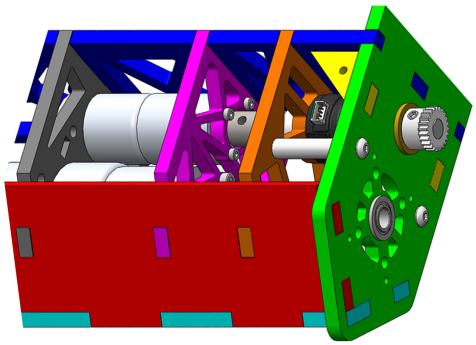

Fig. 5: View of the hip joint. Tab-and-slot construction simplifies assembly and reduces the number of screws required.

V. Prototype

The design goals of the prototype included performance goals (speed, ground clearance, etc.) as well as manufacturability goals (cost, ease of manufacture, etc.).

A. Mechanical Design

The linchpin of this design is the hip joint that pivotally connects each tread assembly to the chassis of the robot. With both motors mounted in the chassis, this joint independently transmits two coaxial torques: one to rotate the sprocket driving the treads and a second to rotate the tread assembly with respect to the chassis. Optical encoders are mounted within the chassis coaxially on both motor shafts. The actuation of the two degrees of freedom on each hip joint enable the robot to perform its unique suite of maneuvers. A set of passive, un-actuated wheels is mounted on the end of the chassis opposite the main drive axles. The wheels prevent the chassis from dragging on the ground when the tread assemblies are rotated higher than the chassis.

The diameter of the sprocket was chosen to give over 25 mm of ground clearance for the chassis when in a horizontal configuration, in conjunction with the motor and gearbox choice to have sufficient torque to lift the weight of the robot, and a top speed in excess of 2.5 m/s (6 body lengths per second). The traction between the treads and various ground surfaces is balanced between the need to grip while accelerating and the need to slip while skid-steering. It is critical to maintain traction while balancing upright, where a tread slipping may cause the robot to fall. The off-the-shelf treads are made of acetal and may be modified by applying a rubberizing coating or adding grousers to increase traction.

Great pains were taken to minimize the part count, particularly the custom part count, and to reduce the number of machining operations per custom part. Off-the-shelf parts were used wherever possible to reduce manufacturing time. All but two of the custom parts are laser-cut from sheets of acetal, with thread-tapping of some holes (thus avoiding the need for nuts) and press-fitting bearings being the only secondary machining operations. The remaining two custom parts are formed from stainless steel rod stock with simple operations on a lathe and milling machine. The symmetry of the design reduces the unique part count and many parts are

orientation-agnostic, simplifying assembly. The 26 unique custom parts account for 73 pieces used in the assembly of each robot, most parts being used in multiple places.

The design process included careful consideration of assembly time. The parts of the superstructure are quickly assembled with a series of interlocking tabs and slots (Fig. 5), thereby minimizing the number of mechanical fasteners needed and saving cost, weight, and assembly time. A team of five undergraduates working under our direction constructed 13 Switchblade robots from part manufacturing to final assembly in 10 weeks.

B. Electronics

Switchblade is built around the National Instruments sbRIO 9602 control board. This board has both FPGA and PowerPC processors, which gives flexibility in handling both low-level high-speed tasks and more complex control algorithms, and is programmed using the LabVIEW graphical programming language, including the Control Design & Simulation and Robotics modules. Built-in ethernet coupled with a wireless ethernet adapter enables real-time wireless communication, debugging, and deployment of software. An AF-1501 frame grabber module from moviMED allows for onboard image processing.

C. Results

Both the simulation and experimental results may be seen in Fig. 6, plotting the critical angles as labeled in Fig. 3. The plot shows a close, though not perfect, correlation between simulation and experiment. The discrepancies may be explained by modeling simplifications and errors; in particular, the motor parameters are not particularly well characterized, and bias error in the measurement of the accelerometer could affect the drift of ϕ. Notably, the robot actually upright faster in the experiment than in simulation. The accompanying video shows the robot performing the uprighting maneuver as in Fig. 4.

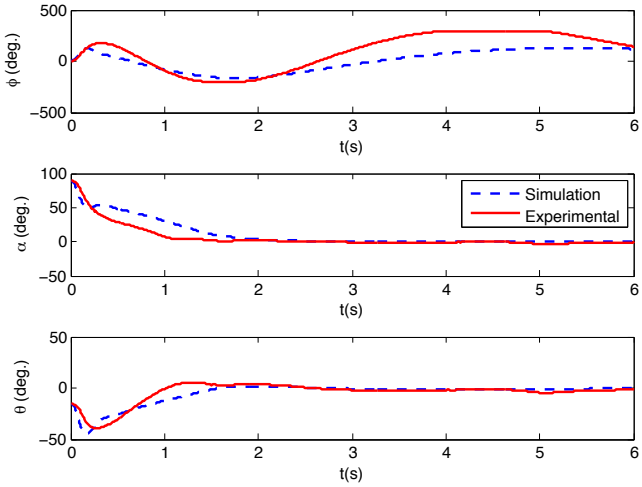

Fig. 6: Comparison of simulation results and experimental results for the Switchblade uprighting maneuver.

VI. Conclusions

A novel robotic platform has been presented which combines the treads of a tank with the balancing behavior of an inverted pendulum to reach a new level of agility. The robot can overcome obstacles on the order of its length instead of the order of its height. A two-degree-of-freedom hip joint enables the current prototype to perform complicated maneuvers with a relatively simple internal structure and wiring. A working prototype has been created that can "stand up" on its own and maintain its balance. This platform has potential for applications in search & rescue, mine exploration, homeland security, border patrol, reconnaissance, and ordnance disposal.

Future work on this platform includes enabling new maneuvers by designing controllers to stabilize statically unstable modes and adding programming to transition seamlessly between different modes of operation, including gracefully recovering from falls. Further control systems implemented will be presented in future papers. Integrating a vision system will enable obstacle detection, namely stairs, to improve the situational awareness of the robot. The final goal is being able to automatically transform to the appropriate configuration based on the terrain encountered.

Acknowledgments

The authors would like to thank National Instruments and moviMED for their generous support, M. Fox for inspiration on the transformable robot concept, and numerous members of the Coordinated Robotics Lab for their assistance in developing the Switchblade prototypes.

References

[1] Segway Inc. http://www.segway.com/
[2] F. Grasser, A. D'Arrigo, S. Colombi, and A. Rufer, "Joe: A mobile, inverted pendulum," *IEEE Trans. Ind. Electron.*, vol. 49, no. 1, pp. 107-114, Feb. 2002.
[3] K. Pathak, J. Franch, S. Agrawal. "Velocity and position control of a wheeled inverted pendulum by partial feedback linearization," *IEEE Trans. Robotics*, vol. 21, no. 3, pp. 505-513
[4] T. B. Lauwers, G. A. Kantor, R. L. Hollis, "A dynamically stable single-wheeled mobile robot with inverse mouse-ball drive," *Proc. ICRA 2006*, pp. 2884-2889, 2006.
[5] M. Kumaga, T. Ochiai, "Development of a robot balanced on a ball," *Proc. ICRA 2009*, pp. 4106-4111, 2009.
[6] T. Sugihara, Y. Nakamura, H. Inoue, "Realtime humanoid motion generation through ZMP manipulation based on inverted pendulum control," *Proc. ICRA 2002*, pp. 1404-1409, 2002.
[7] J. Chestnutt, J. Kuffner, K. Nishiwaki, S. Kagami, "Planning Biped Navigation Strategies in Complex Environments," *Proc. IEEE Int'l. Conf. Hum. Rob.*, pp. 3091-3916, 2003.
[8] C. Schmidt-Wetekam, D. Zhang, R. Hughes, T. Bewley, "Design, optimization, and control of a new class of reconfigurable hopping rovers," *Proc. IEEE Conf. on Decision and Control*, pp. 5150-5155, 2007.
[9] B. Yamauchi, "PackBot: a versatile platform for military robotics," *Proceedings of SPIE*, vol. 5422, pp. 228-237, 2004.
[10] F. Michaud, D. Letourneau, M. Arsenault, Y. Bergeron, R. Cadrin, F. Gagnon, M. Legault, M. Millette, J. Pare, M. Tremblay, P. Lapage, Y. Morin, J. Bisson, S. Caron, "AZIMUT, a leg-track-wheel robot," *Proc. IROS 2003*, pp. 2553-2558, 2003.
[11] J. Borenstein, M. Hansen, "The OmniTread OT-4 serpentine robot-design and performance," *Journal of Field Robotics*, vol. 24, iss. 7, pp. 601-621, 2007.
[12] Vecna Technologies, Inc. http://vecnarobotics.com/solutions/bear/